The Volcanormal Density for Radar-Based Extended Target Tracking

Peter Broßeit
Department for Environment Perception
Daimler AG, Germany
and Institute of Photogrammetry and Remote Sensing, TU Dresden, Germany
Email: peter.brosseit@daimler.com

Bharanidhar Duraisamy
Jürgen Dickmann
Department for Environment Perception
Daimler AG, Germany
Email: bharanidhar.duraisamy@daimler.com, juergen.dickmann@daimler.com

***Abstract*—This paper presents a novel shape model for radar-based vehicle tracking. This model is a special probability density function (pdf), designed to approximate the radar measurement spread of a vehicle more adequately than widely used models. While this pdf is used to determine the likelihood of the spatial measurements, additionally a recent Doppler measurement model is integrated in a maximum likelihood estimator. This formulation allows the estimation of a vehicle's pose, motion and axis lengths based on the radar's spatial and Doppler dimension. On this basis, an efficient computation method is derived. An evaluation of actual radar and ground truth data demonstrates the precise estimation of a vehicle's state.**

I. Introduction

The safe operation of an autonomous-driving vehicle is highly dependent on the quality of the environment model. Especially the dynamic objects in the vehicle's surroundings are a major threat to safety. To avoid collisions, the state of these objects has to be estimated in real-time, based solely on the vehicle's sensor data. Driven by rising vehicle automation and the coupled improvement of sensor technology, such *object tracking* methods face demanding requirements.

Due to the increased resolution of latest automotive radars, multiple reflections per object and measurement cycle are received. In contrast to this, established Bayesian tracking approaches assume a *point target* that reflects at least a single measurement. The development of appropriately enhanced methods, known as *extended target tracking*, has seen tremendous progress over the last years. A comprehensive overview of this topic and bibliography is given by Granström et al. [1]. A crucial component of Bayesian extended object tracking is the shape model and the related link between the measurements and the model. These shape models are based on certain assumptions regarding the characteristics of the respective sensor and the target object type. An important distinctive feature is whether measurements are reflected by the object's contour or surface. Another is the generalization of the model, from specific geometric shapes to arbitrary object models.

However, the representation of a vehicle in high resolution radar measurements conforms not to a clear model as illustrated by Fig. 1. As shown the reflections correspond not to a surface or contour model, but to a mix of both.

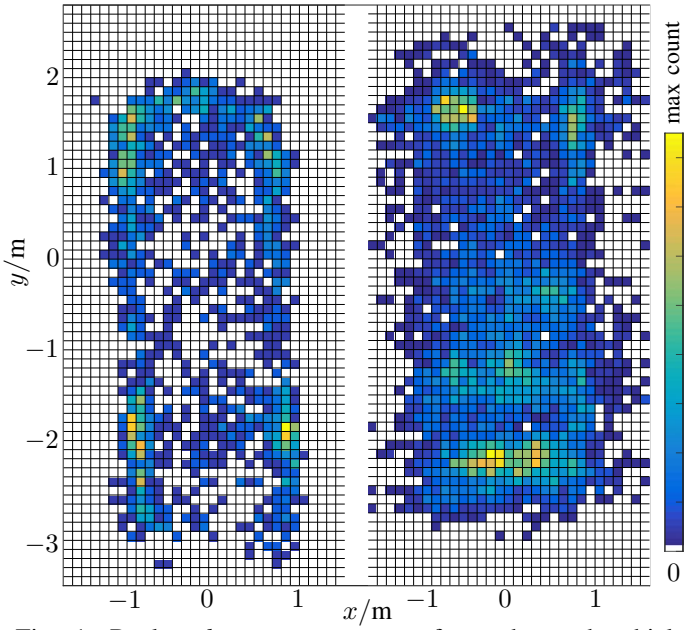

Fig. 1: Real *radar* measurements of an observed vehicle aggregated over time. Using precise localization units, the data is projected in an object-centric coordinate system. The data on the *left* is from a right turn scenario (7.6 s). The grid on the *right* is created from a city traffic scene (47.0 s) where the observed vehicle was driving ahead. The cell size is 0.1 m.

While the strong reflection centers at the vehicle's contour cause the most measurements, a non-negligible amount is also received from the surface. Moreover, the emergence and position of prominent reflection centers depend greatly on the aspect angle, distance and velocities. Note that both grids are aggregated over many seconds - in an automotive application the full state has to be estimated practically immediately once the vehicle has entered the sensor's field of view. This makes it even harder to rely on assumptions regarding scattering centers.

Very well studied in the field of extended object tracking are the *Random Matrix Model* [2] and *Random Hypersurface Model* [3]. The progress of both models is shown in [1] in

978-1-5386-1526-3/17/$31.00 ©2017 IEEE

detail. However, the common assumptions regarding the mode of the measurement spread, which is the object center or equal in a specific region, make these models inapplicable for high-resolution automotive radar-based vehicle tracking as described above. In contrast, they work well for pedestrians and bicycles due to other reflection characteristics. Another drawback for radar applications is that these methods do not use the Doppler measurements.

A more radar-driven approach is the direct modeling of discrete reflection centers as in [4], [5]. With these methods the number, position and arrangement of discrete measurement sources is estimated. Therefore, these methods depend on a clear emergence of these distinct reflection centers. However, in Fig. 1 it can be seen that radar measurements are more complex in practice.

The direct scattering model presented in [6] is related. Rather than distinct reflection centers, it is assumed that the reflections arise along the visible sides of a rectangular object. The measurement likelihood is modeled for each actual reflection based on a ray along the measurement angle. Together with the Doppler likelihood, this model is applied to a Rao-Blackwellized particle filter, which is used for state estimation.

This paper contributes a *probability density function* intentionally designed to approximate the contour-surface-mixed characteristic of a vehicle as measured by automotive radar sensors. Additionally, Doppler measurements are integrated to improve not only the kinematic state estimates, but also position and orientation accuracy. The model couples movement and object orientation, which is appropriate for vehicles.

The structure of this paper is as follows: Section II formulates the problem and prerequisites. In Section III the shape and Doppler model are derived. An efficient estimation method based on this model is introduced in Section IV and evaluated on real-world sensor data in Section V. The conclusion in Section VI summarizes the most important contributions of this paper.

II. Problem Formulation

This paper addresses the estimation of the state of an *observed vehicle* (OV) based on one or more radar sensors mounted on an *ego-vehicle* (EV). The reference pose is the OV's rotation center position and the heading direction (yaw) $\boldsymbol{x} = [x_R, y_R, \alpha]^\mathsf{T} \in \mathbb{R}^3$. The kinematic state composes the scalar velocity in the heading direction and the yaw rate $\boldsymbol{k} = [v, \omega]^\mathsf{T} \in \mathbb{R}^2$. While all these parameters are variable in time, the shape parameters $\boldsymbol{s} = [l, w]^\mathsf{T} \in \mathbb{R}^2$ are constant for a rigid body like a vehicle. In order to meet the application requirements, a system with a constant datum with respect to the EV should be selected as the coordinate system for these parameters. The known pose of each sensor in this system is given by $[x_s, y_s, \gamma_s]^\mathsf{T} \in \mathbb{R}^3$. The overall state has to be estimated for each measurement cycle with temporal index t. The radar sensors resolve N_t measurements with a position and a Doppler velocity $\boldsymbol{z}_i = [\boldsymbol{p}_i, v_{Di}]^\mathsf{T} = [x_i, y_i, v_{Di}]^\mathsf{T} \in \mathbb{R}^3$, where i is an index over N_t. All measurements of a single time stamp t are concatenated in the matrix $\boldsymbol{Z}_t \in \mathbb{R}^{3 \times N_t}$.

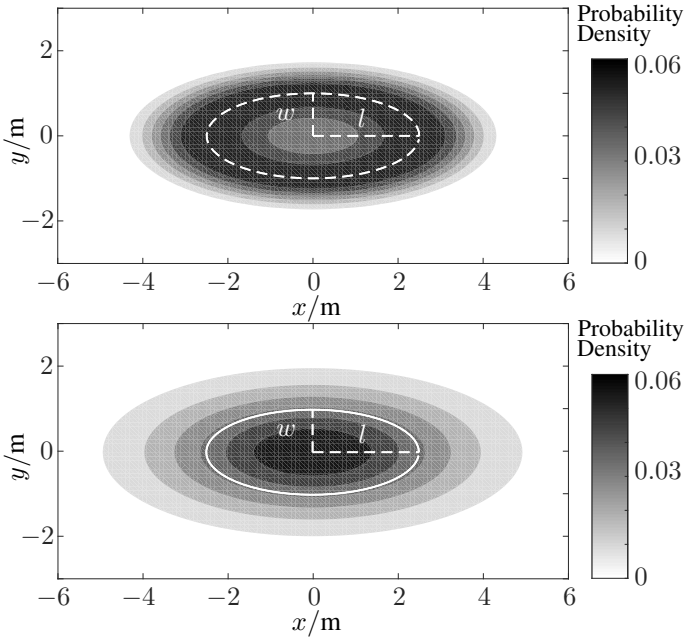

Fig. 2: The proposed *pdf* used for the spatial measurement model (top) compared with a *2d-Gaussian distribution* (bottom). Both distributions are parametrized with zero mean and a diagonal covariance matrix with diagonal entries $l^2 = 2.5^2$, $w^2 = 1^2$.

III. Measurement Models

The measurement model is comprised of two components. One component models the probability density of the spatial measurements, while the second describes the transformation between the state space and the Doppler measurement space.

A. Spatial Component

For the spatial model, a *probability density function* is derived, to approximate the representation of the OV in the radar measurement space. The underlying shape is an ellipse described by a symmetric positive definite matrix, comparable to that of the *Random Matrix Model* [2]. This *spd* matrix is directly set up from the OV's length, width and orientation. The shape parameters specify the spread along the respective axis, without any correlation. The orientation is used to rotate this covariance matrix in the coordinate system of the ego-vehicle.

$$\boldsymbol{\Sigma}_S = \begin{pmatrix} \cos\alpha & -\sin\alpha \\ \sin\alpha & \cos\alpha \end{pmatrix}^\mathsf{T} \cdot \begin{pmatrix} l^2 & 0 \\ 0 & w^2 \end{pmatrix} \cdot \begin{pmatrix} \cos\alpha & -\sin\alpha \\ \sin\alpha & \cos\alpha \end{pmatrix} \tag{1}$$

With the center of the observed vehicle at $\boldsymbol{\mu_M} = (x_M, y_M)$, a *Multivariate Normal distribution* could be used for the measurement model.

$$f = \frac{1}{2\pi \cdot \sqrt{\det(\Sigma_S)}} \cdot \exp\left(-\frac{1}{2} \underbrace{(x_i - \mu_M)^\mathsf{T} {\Sigma_S}^{-1} (x_i - \mu_M)}_{d^2} \right) \tag{2}$$

Where d is the *Mahalanobis distance*. However, the radar measurements are not normally distributed around the center.

To achieve a better approximation of the measurements, the distance d is modified to match the requirements. One requirement is that the highest probability density is on the contour of the object, not the center. This can be achieved by setting $\hat{d} = (d^2 - 1)$, because d equals 1 only for points on the object's contour due to the parametrization of $\mathbf{\Sigma}_S$. Because l and w are used as standard deviations in $\mathbf{\Sigma}_S$, they conveniently weight d. This leads to $-1 \leq \hat{d} < \infty$, where points with $\hat{d} \leq 0$ lying inside the contour. To ensure positive values and increase the slope of the resulting function, $\hat{d}^2$ is used as a substitution for d^2. To once more obtain a valid *pdf* the changed exponential function has to be integrated:

$$\int_{-\infty}^{\infty} \exp\left(-\frac{1}{2}\left((\boldsymbol{p_i} - \boldsymbol{\mu_M})^\mathsf{T} \boldsymbol{\Sigma_S}^{-1} (\boldsymbol{p_i} - \boldsymbol{\mu_M}) - 1\right)^2\right) dxdy$$
$$= \sqrt{\frac{\pi}{8}}\left(\operatorname{erf}\left(\frac{1}{\sqrt{2}}\right) + 1\right) 2\pi\sqrt{\det(\boldsymbol{\Sigma_S})} = \eta \cdot 2\pi\sqrt{\det(\boldsymbol{\Sigma_S})} \tag{3}$$

Where erf is the *Gaussian error function*. The normalization term is the same as for the 2-dimensional *Normal distribution*, despite the constant factor $\eta = 1.0544\ldots$ The resulting *pdf* is given by

$$p(\boldsymbol{p}_i|\boldsymbol{x}_t, \boldsymbol{s}) = \frac{\exp\left(-\frac{1}{2}\left((\boldsymbol{p}_i - \boldsymbol{\mu_M})^\mathsf{T} \boldsymbol{\Sigma_S}^{-1} (\boldsymbol{p}_i - \boldsymbol{\mu_M}) - 1\right)^2\right)}{\eta \cdot 2\pi\sqrt{\det(\boldsymbol{\Sigma_S})}} \tag{4}$$

Fig. 2 shows the resulting *pdf* and an ellipse with axes lengths l, w. With the mode lying on the contour i.e. the underlying ellipse, a strong slope to the outside and a non-vanishing probability density inside, this function can be seen as a sufficient approximation of the spread of radar reflections from an OV. To parametrize the function with the introduced state parameters, $\boldsymbol{\mu_M}$ is set to

$$\boldsymbol{\mu_M} = \begin{pmatrix} x_R + s \cdot \cos\alpha \\ y_R + s \cdot \sin\alpha \end{pmatrix} \tag{5}$$

with the rotation center (x_R, y_R) and an offset s along the orientation α.

B. Doppler Component

The Doppler measurements depend on the OV's pose and kinematic parameters:

$$h(\boldsymbol{x}_t, \boldsymbol{k}_t, \theta_i) = \underbrace{\omega\left((y_R - y_s) \cdot \cos(\theta_i) + (x_s - x_R) \cdot \sin(\theta_i)\right)}_{\omega\text{–component}} + \underbrace{v \cdot \cos(\theta_i - \alpha)}_{v\text{–component}} \tag{6}$$

with the sensor position (x_s, y_s) and measurement angle θ_i. This model is originally derived in [7], based on the work of [8] and also used by [6]. If the sensor orientation γ_s is not aligned with the EV coordinate system, the θ_i arguments have to be substituted by $\theta_i + \gamma_s$, which conforms a rotation of the terms into the sensor system. Then this model is also valid when the parameters are given in the EV coordinate system. With the sensor's standard deviation of the Doppler σ_{v_D} the probability density of the measurements is modeled as Gaussian, similarly as in [6]:

$$p(v_{Di}|\boldsymbol{x}_t, \boldsymbol{k}_t, \theta_i) \sim \mathcal{N}(v_{Di}; h(\boldsymbol{x}_t, \boldsymbol{k}_t, \theta_i), \sigma_{v_D}^2) \tag{7}$$

IV. State Estimation

To apply the models from Section III to state estimation, the problem is formulated in terms of *Maximum Likelihood Estimation*.

A. Likelihood

The *likelihood* of a single measurement $\boldsymbol{z}_i$ is modeled as the product of (4) and (7):

$$\mathcal{L}(\boldsymbol{x}_t, \boldsymbol{k}_t, \boldsymbol{s}, s|\boldsymbol{z}_i) = p(v_{Di}|\boldsymbol{x}_t, \boldsymbol{k}_t, \theta_i) p(x_i, y_i|\boldsymbol{x}_t, \boldsymbol{s}, s) \tag{8}$$

Assuming identical independent distributed measurements, the likelihood of N_t measurements is defined by the product of (8) over N_t. If consecutive timestamps T are considered, only two additional parameters have to be added for each additional time stamp. This is because the shape parameters $\boldsymbol{s}$ as well as the center offset s are constant by definition. Moreover, additional poses are directly determined by the kinematic parameters v and ω from previous poses using the common *constant turn model with polar velocity* [9]:

$$\boldsymbol{x}_t = g(\boldsymbol{x}_{t-1}, v_{t-1}, \omega_{t-1})$$
$$= \begin{bmatrix} x_{R_{t-1}} + \frac{2}{\omega_{t-1}} v_{t-1} \sin\left(\frac{\omega_{t-1}\Delta_t}{2}\right) \cos\left(\alpha_{t-1} + \frac{\omega_{t-1}\Delta_t}{2}\right) \\ y_{R_{t-1}} + \frac{2}{\omega_{t-1}} v_{t-1} \sin\left(\frac{\omega_{t-1}\Delta_t}{2}\right) \sin\left(\alpha_{t-1} + \frac{\omega_{t-1}\Delta_t}{2}\right) \\ \alpha_{t-1} + \omega_{t-1}\Delta_t \end{bmatrix} \tag{9}$$

Therefore, one pose is sufficient to parametrize the full path of the observed vehicle. So for T timestamps the full state $\boldsymbol{\zeta}_{1:T}$ is given as

$$\boldsymbol{\zeta}_{1:T} = \left[x_{R1}, y_{R1}, \alpha_1, l, w, s, v_1, \omega_1, \ldots, v_T, \omega_T\right]^\mathsf{T} \tag{10}$$

And the overall *likelihood* is

$$\mathcal{L}(\boldsymbol{\zeta}_{1:T}|\boldsymbol{Z}_1, \ldots, \boldsymbol{Z}_T) = \prod_{t=1}^{T} \prod_{i=1}^{N_t} p(v_{Di}|\boldsymbol{x}_t, \boldsymbol{k}_t, \theta_i) p(x_i, y_i|\boldsymbol{x}_t, \boldsymbol{s}, s) \tag{11}$$

The *maximum likelihood* of (11) can be estimated by minimizing the *negative log likelihood*, omitting the constant terms:

$$
\begin{aligned}
-\log \mathcal{L}\left(\dots\right) &= \sum_{t=1}^{T}\sum_{i=1}^{N_t}(-\log p(v_{Di}|\boldsymbol{x}_t,\boldsymbol{k}_t,\theta_i) \\
&\quad -\log p(x_i,y_i|\boldsymbol{x}_t,\boldsymbol{s},s)) \\
&= \frac{1}{2}\sum_{t=1}^{T}\sum_{i=1}^{N_t}\left(\left(\frac{v_{Di}-h(\boldsymbol{x}_t,\boldsymbol{k}_t,\theta_i)}{\sigma_{v_D}}\right)^2 + \right. \\
&\left.\left((\boldsymbol{p_i}-\boldsymbol{\mu_M})^{\mathsf{T}}{\boldsymbol{\Sigma_S}}^{-1}(\boldsymbol{p_i}-\boldsymbol{\mu_M})-1\right)^2+\ln\det(\boldsymbol{\Sigma_S})\right)
\end{aligned}
\tag{12}
$$

Where each pose $\boldsymbol{x}_t$ is calculated from $\boldsymbol{\zeta}_{1:T}$ using the motion model (9). Following the *MLE* of $\boldsymbol{\zeta}_{1:T}$ equals the minimization of the three terms in (12). This is a least-squares optimization of the Doppler errors and the distances from the object's contour. The remaining normalization portion has no time dependency, because $R^{\mathsf{T}}\cdot\Sigma\cdot R$ is a *similarity transformation* and

$$\det(\Sigma_S)=\det(R^{\mathsf{T}}\cdot\Sigma\cdot R)=\det(\Sigma)=l^2\cdot w^2.$$

The main potential of this formulation is the integrated exploitation of the Doppler and the spatial measurement dimension. A direct estimation of $\boldsymbol{x}_t$ and $\boldsymbol{k}_t$ based only on (6) is not feasible due to ambiguity in the parameters. However, in (12) the estimation of the pose is directly constrained by the spatial measurement spread. Similarly, the estimation of the poses based on the spatial component is constrained by the Doppler model. Moreover, it can be expected that the joint estimation of the complete state also increases the accuracy of the kinematic and shape parameters. An analysis of the relation between an OV's pose and kinematic state is given in [7]. The offset s between the shape center and the rotation center should be limited to a reasonable range.

B. Ego Motion

If the sensors are mounted on a moving vehicle, the ego motion has to be considered. This is done by using the vehicle's odometry to transform all measurements that should be used for the *MLE* in the ego coordinate system of the last time stamp T. Concerning the Doppler measurement model (6), the sensor positions must also be transformed into this coordinate system. Further, the Doppler measurements are compensated by the ego-motion component in order to obtain the Doppler over ground, see [8].

C. Adjustment calculation

The minimization of (12) can be performed with general optimization methods e.g. a Quasi-Newton method. However, due to the dedicated structure, i.e. quasi least squares problem, a more efficient weighted least squares method is applied [10]. Therefore an equation system has to be set up for the residuals ν which express the discrepancy between the parameter space and the measurements. Each measurement $\boldsymbol{z}_i$ contributes one Doppler equation and one spatial equation to this system, as given directly by (12). Another equation corresponds to the

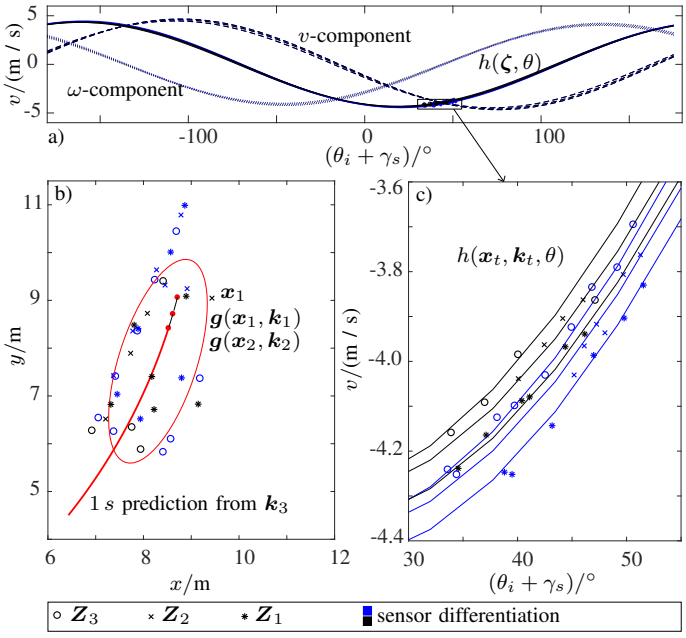

Fig. 3: The relation between the state and measurement space for an estimation based on three consecutive time frames. Fig. 3 a) shows the measurements along with the estimated Doppler profiles (Eq. 6), which is focused in Fig. 3 c). The different curves result from the different parameters. In 3 b) the estimated ellipse is illustrated with the spatial measurements. The two measurement spaces are connected through the kinematic parameters and poses.

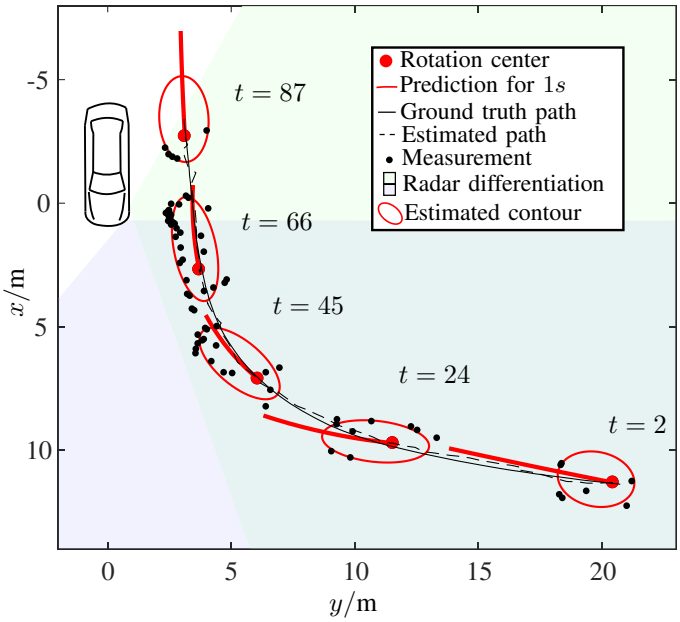

Fig. 4: Scenario 1: The OV is turning right while the EV is standing still at $(0,0)$. The ground truth path and the estimated path are shown together with the estimates for certain positions and the corresponding measurements.

third term $\ln(l^2 w^2)$ with the weight $w_a = \sum_{t=1}^{T} N_t$. Instead of setting the pseudo observation for this equation to 0, it is set to an a priori more reasonable value μ_a because the axis lengths are greater than zero. Another equation is added to limit the bound of the offset s, which for any vehicle is limited to a few meters. Hence it is modeled as a normal distribution with mean μ_s and an appropriate deviation σ_s, which determines the weight. So the overall system comprises $w_a + 2$ rows:

$$\begin{bmatrix} v_{Di} \\ 1 \\ \vdots \\ \mu_a \\ \mu_s \end{bmatrix} - \begin{bmatrix} h(\boldsymbol{\zeta}_{1:T}, \theta_i) - \nu_{t,i}^{v_D} \\ d(\boldsymbol{\zeta}_{1:T}, \boldsymbol{p}_i)^2 - \nu_{t,i}^{p} \\ \vdots \\ 2\ln(l \cdot w) - \nu^a \\ s - \nu^s \end{bmatrix} = 0 \qquad (13)$$

Based on this system and the weights, $\boldsymbol{\zeta}_{\text{opt}}$ can be calculated via weighted least squares regression, see [10] for details. In Fig. 3, estimated parameters are shown along with the measurement data. Data from three consecutive time stamps is used for these estimates.

V. Experimental Results

For the evaluation an experimental vehicle equipped with four radar sensors was used. In two different scenarios the state of an observed vehicle was estimated by the proposed adjustment method (IV-C). Additionally, the position, orientation and motion of both vehicles is constantly measured using a *Differential Global Navigation Satellite System* and an *Inertial Measurement Unit*, providing ground truth data for the evaluation. The used 77 GHz radar sensors were mounted around the bumper, oriented 25° and 85° from the longitudinal axis to both sides. The measurement cycle is roughly 60 ms.

A *RANSAC* [11] method was applied to remove outliers, based only on the Doppler model (6) to increase the computation performance. All remaining measurements were used with the estimation, which is computed in each time step from the current and the last four measurement frames. Even if each motion parameter set $\boldsymbol{k}$ is computed multiple times, due to the sliding window processing of $\boldsymbol{\zeta}$, only the most recent estimate $\boldsymbol{k}_t$ is considered in the evaluation because this is the most relevant for the environment model. The offset parameters are set to $\mu_s = 0.7$ and $\sigma_s = 0.3$ while the shape parameter μ_a was set to 1.1. Both means are intentionally different from the true values, which are $\mu_s = 1.3$ and $\mu_a = 1.9$ for the used OV.

In the first scenario, the EV is standing at an intersection while the OV is approaching from the left and turning right to pass the EV as shown by Fig. 4. The accuracy is illustrated in Fig. 5 by the process of the current parameter errors and the axis lengths while the overall root-mean-square errors are summarized in Table I. From the figures it can be seen that overall a good accuracy is achieved without large outliers. Additionally, the standard deviation that is estimated by the adjustment calculation reflects the uncertainty for each parameter. It is remarkable that even when the measurement spread

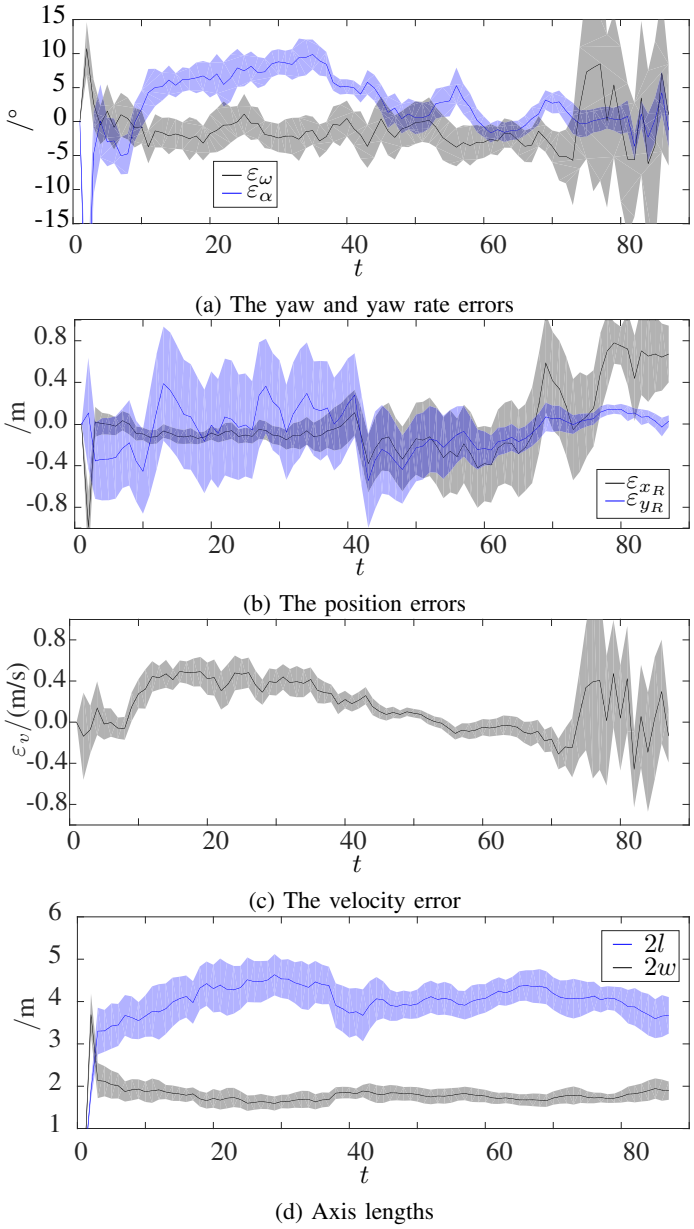

(a) The yaw and yaw rate errors

(b) The position errors

(c) The velocity error

(d) Axis lengths

Fig. 5: The parameter errors and the axis lengths. In addition the standard deviation as estimated by the adjustment computation method is depicted for each parameter and time index.

does not represent the whole shape, because only the vehicle's rear or side is observed, a good estimate of the axis lengths and rotation center position is still achieved. This is possibly due to the adequate measurement spread model (4) and the integrated processing of the Doppler. However, when only a small part of the OV is observed the errors will increase, as can be seen at the end of the scene in Fig. 5.

The second scenario is a city traffic scene, where the OV overtakes the EV at the beginning to drive ahead through a multi-lane roundabout (Fig. 6). In this scene, the ego-motion is an additional error source but a good estimation accuracy could still be achieved. Both scenarios together demonstrate

TABLE I: RMS-Errors of the estimated state parameters

Parameter		$\in \boldsymbol{\zeta}$	Scenario 1	Scenario 2
Position	/m	x	0.32	0.78
		y	0.22	0.45
Orientation	/°	α	4.67	3.65
Velocity	/m/s	v	0.30	0.15
Yaw rate	/°/s	ω	3.65	2.97

that it is feasible to estimate the full state of the OV using the proposed model from 5 measurements, corresponding to $4 \cdot 60$ ms. Using more previous measurements would directly lead to a slightly improvement of the accuracy as shown in Fig. 7 for scenario 1. However, a larger window size impairs the runtime performance.

VI. Conclusion

This paper presented a probability density function intentionally designed to model a vehicle's appearance in the radar measurement space. Through combination with an appropriate Doppler model, an estimator was formulated that depends jointly on the spatial and Doppler dimension. Processing data from multiple radar sensors is directly applicable. In the experiments, the full state was estimated with an overall high accuracy and without substantial outliers. This is seen as evidence that the proposed model is indeed a sufficient approximation of the radar measurement spread. Subsequent work is planned to integrate the model in Bayesian filtering frameworks.

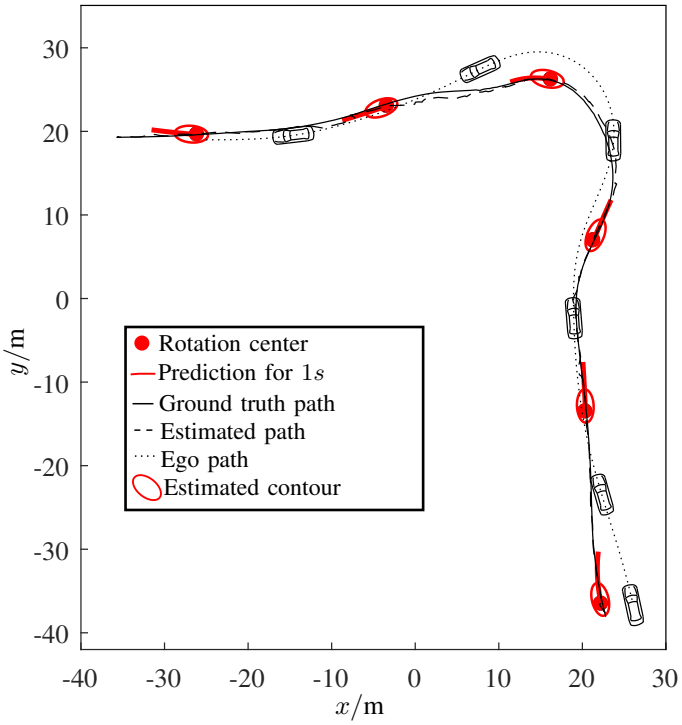

Fig. 6: Scenario 2: The path of the EV (dotted) along with the estimated path of the OV (dashed) and the related ground truth (solid).

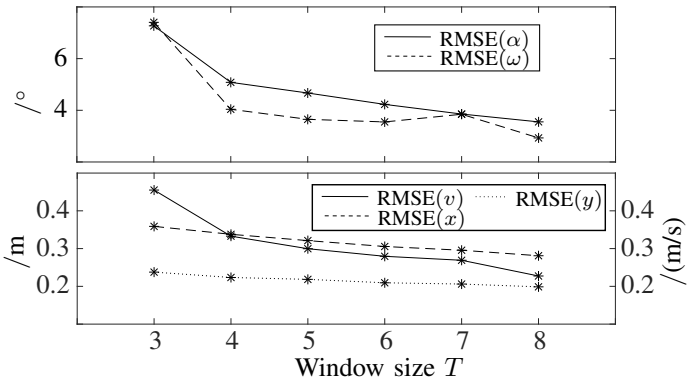

Fig. 7: The influence of the number of used measurement cycles on the overall RMSE of scenario 1.

References

[1] Karl Granström, Marcus Baum, and Stephan Reuter. Extended Object Tracking: Introduction, Overview and Applications (to appear). *ISIF Journal of Advances in Information Fusion*, 2017. Preprint available at https://arxiv.org/pdf/1604.00970.pdf.

[2] Wolfgang Koch. Bayesian approach to extended object and cluster tracking using random matrices. *IEEE Transactions on Aerospace and Electronic Systems*, 44(3):1042–1059, 2008.

[3] Marcus Baum, Benjamin Noack, and Uwe D. Hanebeck. Extended object tracking with random hypersurface models. *IEEE Transactions on Aerospace and Electronic Systems*, 50(1):149–159, 2014.

[4] Lars Hammarstrand, Malin Lundgren, and Lennart Svensson. Adaptive radar sensor model for tracking structured extended objects. *IEEE Transactions on Aerospace and Electronic Systems*, 48(3):1975–1995, 2012.

[5] Lars Hammarstrand, L. Svensson, and F. Sandblom. Extended Object Tracking Using Radar Resolution Model. *IEEE Transactions on Aerospace and Electronic Systems*, 48(3):2371 – 2386, 2012.

[6] Christina Knill, Alexander Scheel, and Klaus Dietmayer. A direct scattering model for tracking vehicles with high-resolution radars. In *IEEE Intelligent Vehicles Symposium, Proceedings*, pages 298–303, 2016.

[7] Peter Broßeit, Dominik Kellner, Carsten Brenk, and Jürgen Dickmann. Fusion of Doppler Radar and Geometric Attributes for Motion Estimation of Extended Objects. In *Sensor Data Fusion: Trends, Solutions, Applications*, 2015.

[8] Dominik Kellner, Michael Barjenbruch, Jens Klappstein, and Klaus Dietmayer. Tracking of Extended Objects with High Resolution Doppler Radar. *IEEE Transactions on Intelligent Transportation Systems*, PP(99):1–13, 2015.

[9] X. Rong, Li and V. P. Jilkov. Survey of Maneuvering Target Tracking. Part I. Dynamic Models. *IEEE Transactions on Aerospace and Electronic Systems*, 39(4):1333–1364, 2003.

[10] C. D. Ghilani. *Adjustment Computation - Spatial Data Analysis*. John Wiley & Sons, Hoboken, New Jersey, 2010.

[11] Martin A. Fischler and Robert C. Bolles. Random sample consensus: A paradigm for model fitting with applications to image analysis and automated cartography. *Commun. ACM*, 24(6):381–395, June 1981.